Advanced Composite Materials

ISSN: 0924-3046 (Print) 1568-5519 (Online) Journal homepage: http://www.tandfonline.com/loi/tacm20

Comparison of thermal deformations of carbon fiber-reinforced phenolic matrix ablators by arc-plasma wind tunnel heating and quasi-static heating

Yuki Kubota, Kohei Fukuda, Hiroshi Hatta, Ricarda Wernitz, Georg Herdrich & Stefanos Fasoulas

To cite this article: Yuki Kubota, Kohei Fukuda, Hiroshi Hatta, Ricarda Wernitz, Georg Herdrich & Stefanos Fasoulas (2015) Comparison of thermal deformations of carbon fiber-reinforced phenolic matrix ablators by arc-plasma wind tunnel heating and quasi-static heating, Advanced Composite Materials, 24:2, 179-195, DOI: 10.1080/09243046.2014.882539

To link to this article: http://dx.doi.org/10.1080/09243046.2014.882539

Published online: 05 Feb 2014.

Advanced Composite Materials, 2015
Vol. 24, No. 2, 179–195, http://dx.doi.org/10.1080/09243046.2014.882539

Comparison of thermal deformations of carbon fiber-reinforced phenolic matrix ablators by arc-plasma wind tunnel heating and quasi-static heating

Yuki Kubota[a]*, Kohei Fukuda[b], Hiroshi Hatta[c], Ricarda Wernitz[d], Georg Herdrich[d] and Stefanos Fasoulas[d]

[a]*School of Physical Sciences, The Graduate University of Advanced Sciences, Sagamihara, Japan;* [b]*Material Science and Technology, Tokyo University of Science, Katsushika, Japan;* [c]*Institute of Space Astronautical Science, Sagamihara, Japan;* [d]*Institute of Space System, University of Stuttgart, Stuttgart, Germany*

(*Received 26 September 2013; accepted 9 January 2014*)

Thermal deformation mechanisms of ablators were elucidated using two types of different pore-size materials under quasi-static heating (QS) conditions. When the material has small pores (Material 1), large expansion in the thickness at temperatures higher than 500 °C occurred by buckling of fiber bundles caused by mismatch strain between the fiber and matrix when the matrix shrunk. In contrast, when large pores are included in the matrix (Material 2), the cracking in the matrix relaxed the mismatch strain and suppressed the buckling. Next, the deformation of Material 1 after arc-plasma wind tunnel heating (AP) tests was examined to identify the causes of thermal deformation. In this environment, expansion also occurred. However, in addition to the fiber bundle buckling, delamination leads to larger expansion than that in QS. The temperature generating expansion in AP tests was higher than that in QS tests. This behavior is caused by reaction rate slower than rapid heating rate.

Keywords: word; ablator; deformation; expansion; defect; crack; arc-plasma wind tunnel

1. Introduction

Ablation cooling is a thermal protection method adopted for severe heating environments such as the re-entry of space vehicles into the earth's atmosphere after space explorations. An ablator system covering a space vehicle protects payloads from aerodynamic heating by consumption of ablation material. Gases generated by pyrolysis of the ablator cover the vehicle to insulate it from hot environmental gases. The consequent endothermic decomposition reactions further prevent to increase the material temperature. Low thermal conductivity of the ablator material also contributes to prevent increasing the payload temperature. Carbon fiber-reinforced phenolic matrix composites have been often used as ablation material.[1]

To evaluate performance of ablators, arc-plasma wind tunnel heating (AP) tests have been conducted, in which an ablator material has exposed to high-speed plasma flow possessing extremely high temperature. However, the AP test cannot realize the re-entry environments, because gas flow speed or impact pressure in re-entry

*Corresponding author. Email: kubota.yuuki@ac.jaxa.jp

environments cannot be reproduced by it. Thus, the performance of ablators in re-entry conditions has been evaluated by extrapolating results of AP tests.[2]

When an ablator is exposed to severe environments, the ablator volume decreases by chemical reactions and sublimation at high temperature.[1–3] Thus, the recession of the ablator surface by heating is the key information for designing ablator thickness. To use ablator for re-entry capsule, the recession should not be larger than the ablator thickness, and should be predicted precisely. The recession has been determined by subtracting the thickness after heating from that before heating. In severe high temperature environments, ablators are damaged to produce many cracks. This damage often expanded the ablator as shown in Figure 1,[3] and the expansion is not negligibly smaller than the recession. Therefore, the net recession has not been evaluated precisely, because the expansion of material has been included in measurements of recession. Thus, damage-related deformation at elevated temperatures must be elucidated.

Understanding of damage in an ablator is also important for evaluations of material properties of an ablator. For predictions of temperature distribution and recession, material properties of an ablator, such as thermal conductivity and density, are required. However, these properties sensitively depend on damage in the material. This is another motivation to discuss damaging process of ablators in the present study.

In AP tests, the material is heated unidirectionally and rapidly. Consequently, unsteady rapid-changing temperature distribution with a sharp gradient is induced in an ablator. Under such complex heating conditions, it is difficult to specify the basic mechanisms yielding the expansion deformation and degradation, because observation of the cross-section of material after heating is the only way to assess the damage in AP tests. Therefore, elucidation of the basic mechanisms is crucially important to ascertain deformation behavior.

This study was composed of two parts. In the first step, deformation mechanisms under quasi-static heating (QS) conditions are discussed in relation to degradation. In

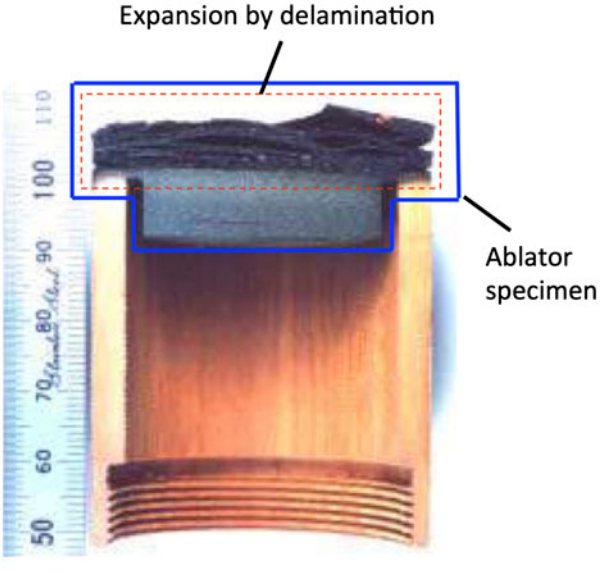

Figure 1. A cross-section of an ablator after an arc-plasma wind tunnel heating.

the QS, the materials were heated slowly with nearly uniform temperature distributions. In the second step, arc-plasma wind tunnel heating (AP) were conducted, and using information obtained in the QS tests, cross-sections of a material after AP were observed to identify causes of thermal deformation under high-speed plasma flow and high-enthalpy conditions.

2. Experiments

2.1. Material

Carbon fiber-reinforced phenolic matrix composites were used as the ablation material. The reinforcement of specimens was an eight satin-weave of kynol-based carbon fiber with a special micro-structure as presented in Figure 2. This structure was formed, at first, spinning short fibers into a thin sub-bundle. Then, three sub-bundles are braided into a yarn. The kynol fiber is suitable for the reinforcement of ablation material, because the thermal conductivity and density is lower than those of general carbon fiber (PAN or pitch-based carbon fiber). Although several researchers have reported thermal deformation of CFRPs reinforced with general type of carbon fibers,[4–6] deformation of kynol-based carbon fiber-reinforced composites has not been investigated. Resol-type phenolic resin has been applied as the matrix of ablation materials because this resin exhibits low recession due to high char yielding.

To elucidate the expansion mechanisms of the ablation materials, specimens having two different porosities and pore sizes (Materials 1 and 2) were manufactured. Figure 3 depicts typical cross-sections of Material 1 (a) and Material 2 (b). The porosities of as-received Material 1 and 2 were 20.9 and 31.0%. Figure 4 compares pore size distributions of Material 1 and 2 in a 10 mm^2 of a cross-sectional area, where the vertical axis stands for number of pores N multiplied by designated area A and horizontal axis A. This figure shows that pores larger than 2.5×10^4 μm^2 are seldom in Material 1 but many in Material 2.

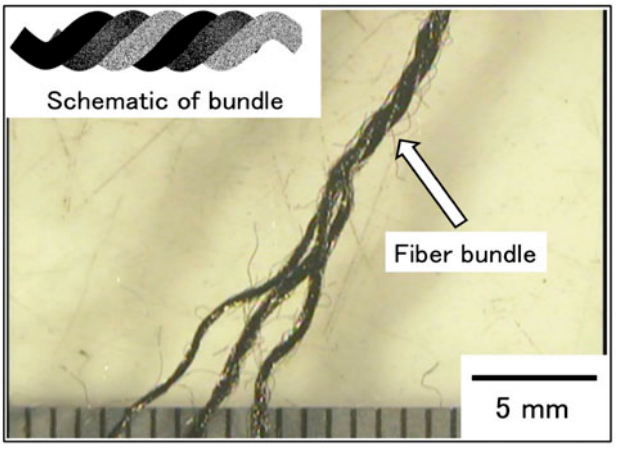

Figure 2. A kynol-based carbon fiber bundle.

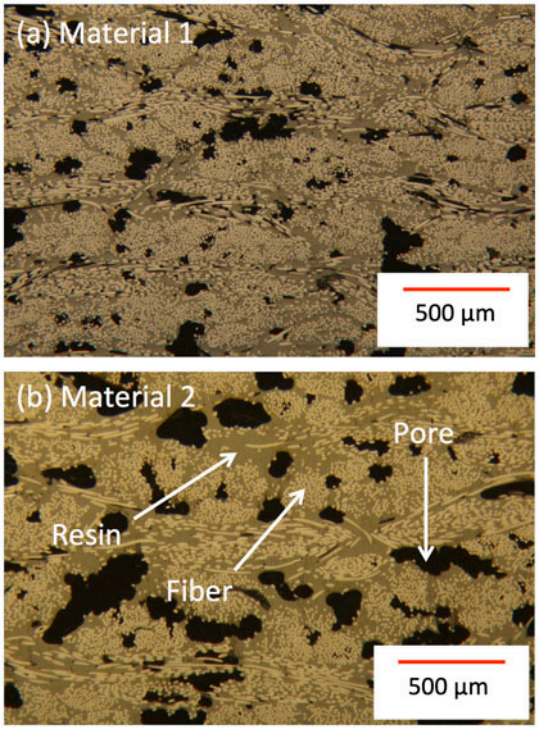

Figure 3. Cross-sections of as-received materials: (a) Material 1 and (b) Material 2.

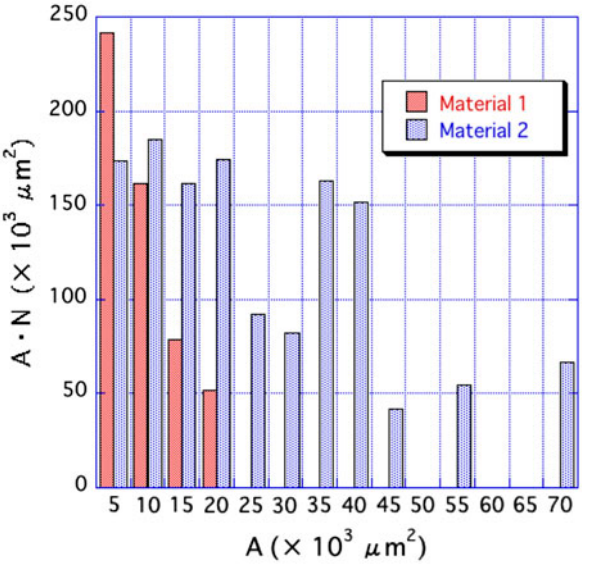

Figure 4. Comparison of pore sizes in Material 1 and 2. The vertical axis represents number of pores N multiplied by the area of single pore A and horizontal axis A.

2.2. Quasi-static heating tests (QS tests)

Thermal deformation under quasi-static heating (QS) was measured using a thermo-mechanical analyzer (TMA, TMA-50; Shimadzu Corp.). Measurements were conducted at 1.0 atm of Ar atmosphere and at heating rates of 1, 10, and 50 °C/min. Deformation was measured in the thickness direction of the laminated composites. The sample size used for these tests was 5.0 mm × 5.0 mm × 7.0 mm.

The development of defects at elevated temperatures under QS environments was *in situ* observed using an optical microscope (BH2-UMA; Olympus Corp., Japan) equipped with a heating furnace (MVH-5; Japan High Tech Co. Ltd.). The specimen geometry was approximately 3.0 mm × 3.0 mm × 3.0 mm. Observations of cross-sectional surfaces of the laminated plates were conducted at a heating rate of 10 °C/min under Ar atmosphere.

2.3. Arc-plasma wind tunnel heating tests (AP tests)

2.3.1. Specimens

Only Material 1 was tested using arc-plasma wind tunnel. Cylindrical specimens depicted in Figure 5 were used for AP tests, where the thickness and diameter of the specimens were 40.0 and 39.8 mm, respectively. The top surface of a specimen was exposed to high-speed plasma flow. In accordance with a re-entry capsule, the lamination plane of the material was inclined by 22.5° to easily release the trapped gases in a specimen, and to avoid spallation of damaged portions.[1]

Five thermocouples (TCs) were inserted into a specimen. The nearest one to the top surface was TC 1; TC 5 was the nearest to the bottom of the specimen. TC 1, TC 3, and TC 5 were inserted to 20 mm depth from the side surface. TC 2 and TC 4 were inserted to 10 and 5.0 mm depths, respectively. The top surface temperature was measured using a pyrometer, where the emissivity of material was assumed to be 0.85.[7]

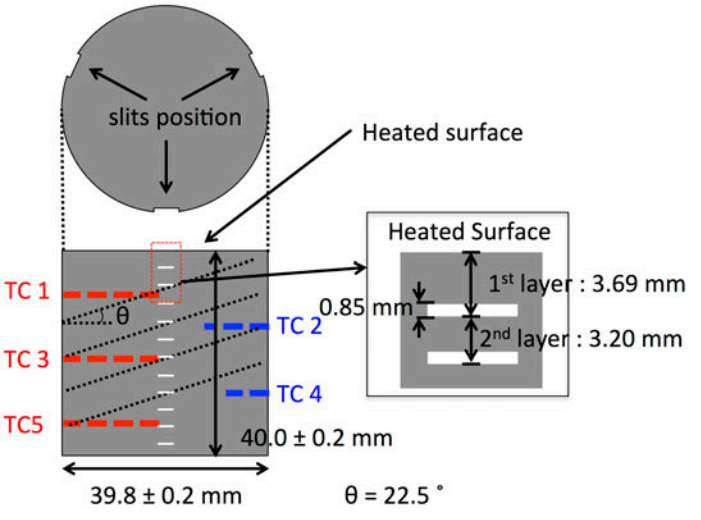

Figure 5. Geometry of specimen for the arc-plasma wind tunnel heating tests.

Three arrays of slits were engraved on the side surface of the specimens to measure the change of spacing between adjacent slits before and after heating. Hereafter, the region from the top surface to the base of the first slit is called the first slit layer, and from the base of the first slit to that of the second one is the second slit layer, and so on, as shown in Figure 5.

2.3.2. *Experimental conditions*

The arc-plasma wind tunnel used for this study was PWK 1 of Institute of Space Systems (IRS) of Stuttgart University.[8] Table 1 presents specifications of PWK 1. This facility features production of high-enthalpy conditions of 2.0–150 MJ/kg together with high-speed plasma flow.

AP tests were conducted at heat fluxes of 2.0, 6.0, or 12.0 MW/m^2. These tests were designated, respectively, as tests *A*, *B*, and *C*. Their respective experimental conditions are presented in Table 2. The heating time in each test differed: 60 s in test *A*, 30 s in test *B*, and 12 s in test *C*. In the experiments, a specimen was put into plasma flow after heat flux of flow field became steady.

2.3.3. *Measurement of deformation*

Thermal deformation of a specimen in the thickness direction was determined from the variation of slit spacings before and after heating. Total thickness variation of specimen was additionally measured using a micrometer.

The lamination planes were inclined at an angle of 22.5° in the AP specimens, and parallel to the top surface in the QS specimens. To compensate this difference, the deformation obtained in the AP tests was corrected using a correction factor of cos 22.5°.

An X-ray CT (Toshiba Corp. Japan) was used for observation of damage inside specimens after heating in the arc-plasma wind tunnel. The maximum resolution of it was 5 μm/pixel. The pixels of observed images were 1024 × 1024.

3. Results

3.1. *Quasi-static heating tests (QS tests)*

3.1.1. *Thermal deformation*

Figure 6 shows thermal deformation of Material 1 and 2 up to 900 °C at a heating rate of 1.0 °C/min. The pyrolysis reaction in phenolic resin starts from 300 to 400 °C and causes resin shrinkage. In the general type of CFRP (reinforced with PAN-based or pitch-based fibers), the thickness of CFRP decreased in conjunction with the resin

Table 1. Specifications of arc-plasma wind tunnel (PWK 1).

Length of tunnel [m]	6.0
Diameter of tunnel [m]	2.0
Bulk enthalpies [MJ/kg]	2.0–150
Total pressure [hPa]	1–100
Working gases	N_2, Ar, O_2, He $N_2 + O_2$, $Ar + O_2$, $N_2 + CH_4$, $Ar + CO_2$
Diameter of nozzle exit [mm]	125

Table 2. Experimental conditions for arc-plasma wind tunnel heating tests.

AP test	*A*	*B*	*C*
Heat flux [MW/m^2] (±10%)	2.0	6.0	12.0
Heating time [s]	60	30	12
Pitot pressure [hPa] (±0.1)	33.2	38.3	43.4
Ambient pressure [hPa] (±0.1)		27	
Total mass flow [g/s] (±0.1)		18.0	
Oxygen mass flow [g/s] (±0.1)		4.2	
Nitrogen mass flow [g/s] (±0.1)		13.8	
Argon mass flow [g/s] (±0.1)		0.5	

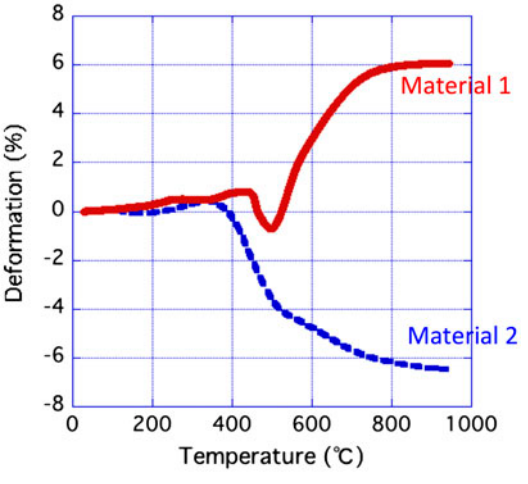

Figure 6. Thermal deformation of Material 1 and 2 measured at a heating rate of 1.0 °C/min.

shrinkage.[4–6] As shown in Figure 6, the deformation behavior of Material 2 accorded with earlier reports; material shrinkage was observed at temperatures higher than 350 °C. However, the deformation behavior of Material 1 shifted from shrinkage to expansion at 500 °C. These materials were not deformed at temperatures higher than 900 °C and during cooling process. The deformations below 500 °C under QS were described in detail in our early paper.[9] The present paper focuses only on the deformations observed at temperatures exceeding 500 °C.

3.1.2. *Thermal degradation*

The shrinkage of resin due to the pyrolysis reactions produces mismatch strain between the fiber and matrix in CFRPs at elevated temperatures, which causes transverse cracks and delamination.[4–6] In the present study, no defect was observed at temperatures lower than 500 °C. Major defects increasing porosity were produced only at temperatures higher than 500 °C, due to active pyrolysis reaction.[9] Therefore, the expansion of Material 1 over 500 °C shown in Figure 6 is expected to be induced by defects produced by the pyrolysis reaction of the phenolic resin.

Figure 7 shows cross-sections of (a) Material 1 and (b) Material 2 observed at 900 °C. As these figures show, the defects were located inside the bundle in Material 1, and in resin-rich regions in Material 2. The difference in thermal deformation at temperatures exceeding 500 °C as portrayed in Figure 6 is most likely caused by differences in defect formation behaviors.

3.1.3. *Sources of deformation*

3.1.3.1. Material 1. Opening of the cracks observed within fiber bundles was determined using graphics software (Photoshop Element 7; Adobe Systems Inc.). Figure 8 symbolically presents the area of a crack inside bundle (painted blue) enlarging with observation temperature. The crack opening to the laminated direction C^T_{open} was calculated from Equation (1).

$$C^T_{open} = \frac{A_T}{L_T}, \tag{1}$$

where L_T and A_T indicate a crack length and crack area at a temperature T as described in Figure 8. This crack opening was normalized by the value at 550 °C.

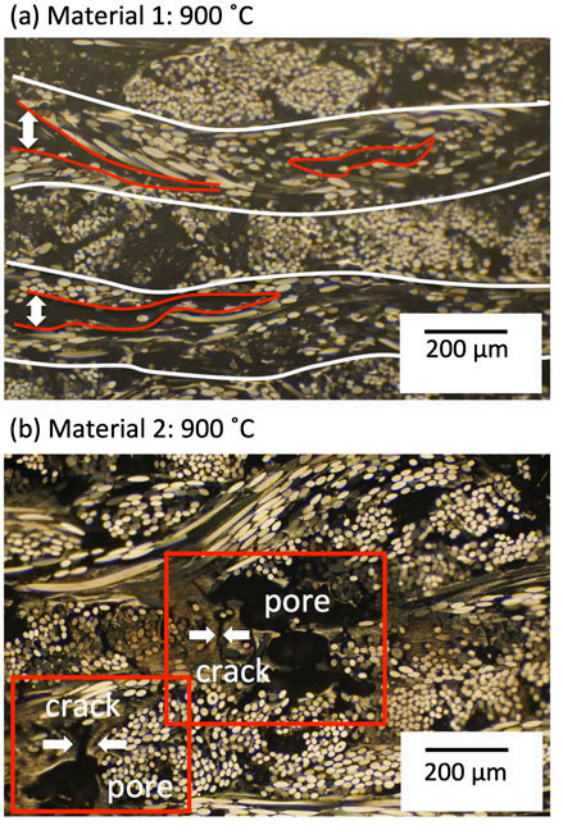

Figure 7. Typical optical micro-photos of cross-sections of (a) Material 1 and (b) Material 2 observed at 900 °C.

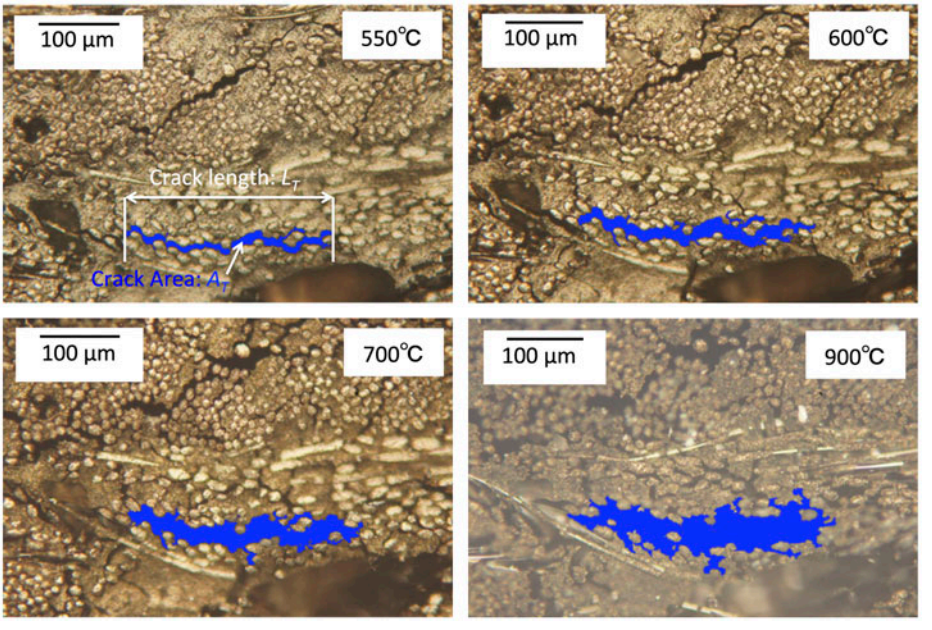

Figure 8. Variation of crack area with observation temperature due to the pyrolysis reaction in Material 1 observed in quasi-static heating condition.

$$R^T_{open} = \frac{C^T_{open}}{C^{550}_{open}}. \tag{2}$$

The reference was taken at 550 °C, because cracks initiated around this temperature. R^T_{open} is compared with normalized expansion R^T_{expa} defined by Equation (3) in Figure 9 as a function of temperature.

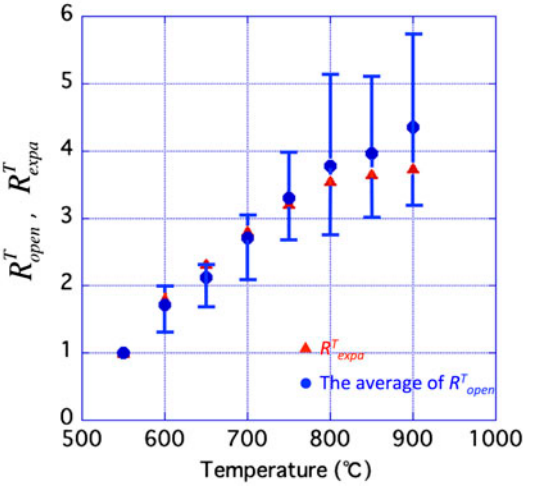

Figure 9. Comparison of normalized expansion of Material 1 observed by TMA R^T_{expa} with normalized crack opening R^T_{open} as a function of temperature from 550 to 900 °C.

$$R^{T}_{expa} = \frac{E_T}{E_{550}}, \tag{3}$$

where E_T stands for the material expansion measured at temperature T. Figure 9 shows that R^{T}_{open} changes consistently with R^{T}_{expa}. This result indicates that the cracks inside bundles are the source of the thickness expansion of Material 1.

Next, optional length of fiber bundles at 550 °C l_{550} described in Figure 10 was measured, and change of the l_{550} at 900 °C was calculated using Equation (4).

$$\Delta l = \frac{l_{900} - l_{550}}{l_{550}} \times 100. \tag{4}$$

Figure 11 shows Δl as a function of R^{900}_{open}. This figure describes that when the crack opening in the thickness direction was larger, then length of fiber bundle became shorter. From the results of Figures 9 and 11, and the fact that the fiber bundles are compressed in the fiber axis direction by the matrix shrinkage during the pyrolysis reaction, the buckling of sub-bundles illustrated in Figure 10 is presumed to be the source of enlarging diameter of fiber bundles.

3.1.3.2. Material 2. Although the same fiber and matrix were used, Material 1 expanded, and Material 2 shrank monotonically at temperatures higher than 500 °C, as observed in Figure 6. The only differences in material constitutions of both materials were the porosity and the pore size. The total porosities of Material 1 and 2 at 600 °C were 49.2 and 50.3%, respectively, being nearly equal. Thus, the major difference is the size of pores at the temperatures exceeding 500 °C.

When the matrix shrinks, tensile stress in the direction of the bundle axis is generated in the matrix. The stress in the matrix beside a pore σ_m as described in Figure 12 is approximately calculated as a function of pore diameter a.

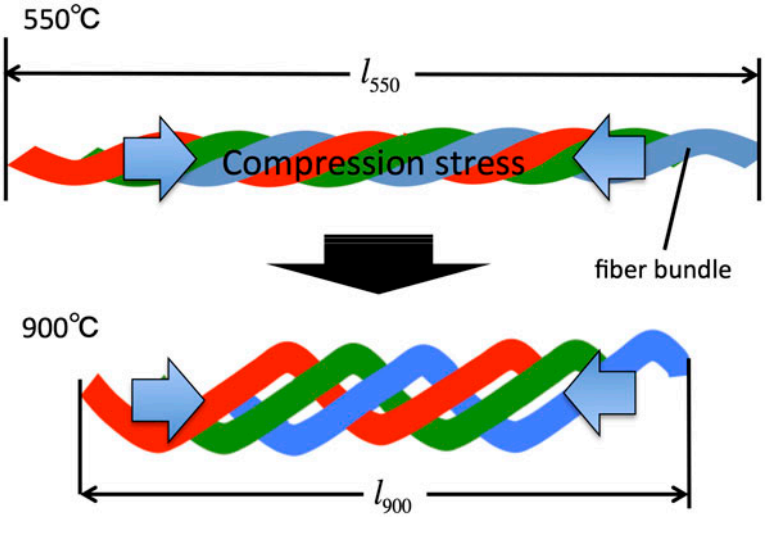

Figure 10. Presumed buckling of a fiber bundle in Material 1.

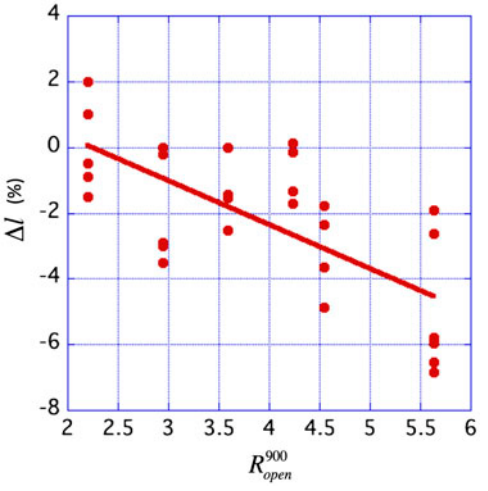

Figure 11. Variation of crack length Δl in Material 1 with normalized crack opening at 900 °C R^{900}_{open}. $R^{900}_{open} > 1$ represents expansion in the thickness.

$$\sigma_m = \frac{P}{b-a} \tag{5}$$

where b and P are width of resin layer and tensile force, respectively. Equation (5) indicates that when pore size is large, σ_m become high. This is likely the principal reason why larger pores induced the matrix cracks in Material 2 as shown in Figure 7(b). Because this type of cracks relaxed the compression stress on the fiber bundles, the buckling as in Material 1 was not likely observed in Material 2. This explains why the thickness of Material 2 shrank according to the shrinkage by pyrolysis of the matrix resin.

3.2. *Arc-plasma wind tunnel heating tests (AP tests)*

3.2.1. *Temperature of specimen*

Figure 13 presents typical temperature histories on the heated surface and inside material in AP test *A*. In this figure, the red curve from 210 to 300 s indicates correct

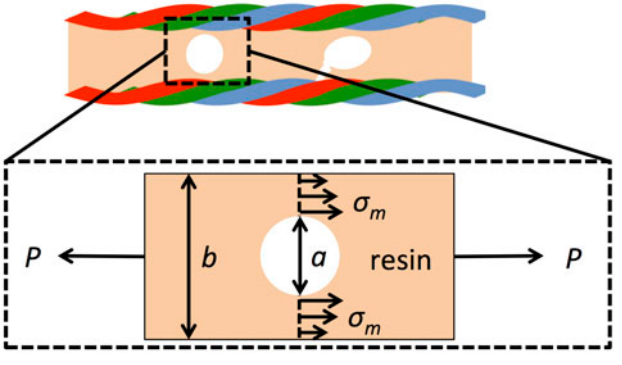

Figure 12. Stress state in the matrix beside a pore.

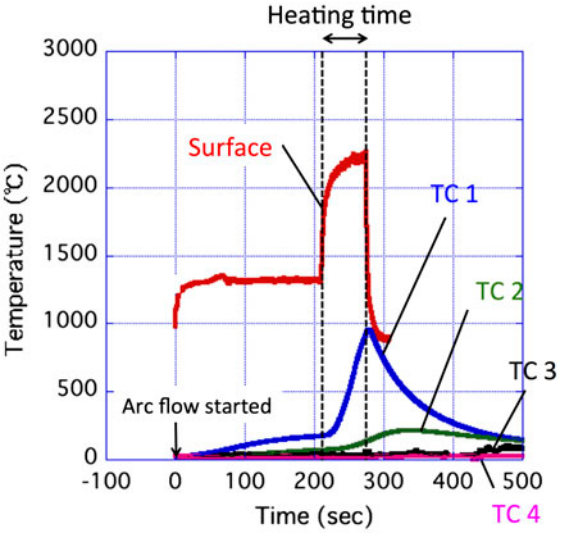

Figure 13. Temperature histories obtained by arc-plasma wind tunnel heating test *A*.

surface temperature. Before the heating time, $t < 210$ s, the pyrometer looked at only flowing plasma gas, not testing material, and after 300 s, temperature is out of range of the pyrometer.

3.2.2. *Thermal deformation*

Table 3 presents the change of total thickness of material measured using a micrometer after the tests. The total thickness of the specimen decreased slightly after test *A*, but increased after tests *B* and *C*.

Deformation distribution was determined from the change of slit layer thickness. The layers below fifth did not deform after any tests. Table 4 shows that the deformation generally increased when a layer approaches the heated surface. However, this rule

Table 3. Average deformation after the arc-plasma wind tunnel heating tests.

AP test	*A*	*B*	*C*
Total deformation (%)	−0.106	+0.723	+1.54

Table 4. Average deformation at first to fourth slit layers after the arc-plasma wind tunnel heating tests (positive values indicate expansion).

AP test		*A*	*B*	*C*
Slit layer	Distance from surface (mm)	Deformation (%)		
1st	0.0–3.69	−6.40	1.77	10.87
2nd	3.69–6.93	3.17	5.23	4.57
3rd	6.93–10.2	1.49	1.83	−0.87
4th	10.2–13.4	0.43	0	−0.43

Table 5. Recession in the arc-plasma wind tunnel heating tests.

AP test	*A*	*B*	*C*
Recession (μm)	575	345	0

is not met in the first slit layers of the tests *A* and *B*, i.e. deformations of the first layers decreased. The heating durations of test *A* and *B* were much longer than that in test *C* (see Table 2). Consequently, the recession caused by the chemical reaction on the surface might be greater than in test *C*. To estimate recessions, the numbers of laminae in the first slit layer N_S before and after the AP tests were counted. Before heating N_0 was 8, and N_1s after tests *A*, *B*, and *C* were 6.75, 7.25, and 8, respectively. Differences between N_0 and N_1s were then converted to the recession as shown in Table 5. If we assume that the recessions shown in Table 5 had not occurred, the average expansions in the first slit layer were calculated as shown in Figure 14 using Equation (6).

$$\Delta d = \frac{d_1 - (d_0 - r)}{(d_0 - r)} \times 100 \tag{6}$$

where r is the recession presented in Table 5, and d_0, d_1 denote thickness of first slit layer before and after the AP tests, respectively. This figure indicates that expansions in the first slit layers during the AP tests were greater than that after the quasi-static heating (QS) tests.

3.2.3. *Thermal degradation*

Figure 15 shows an image of a cross-section after AP test *A* was observed using the X-ray CT. The first and second slit layers become darker, indicating charring. Observations using X-ray CT after tests *B* and *C* revealed a similar tendency.

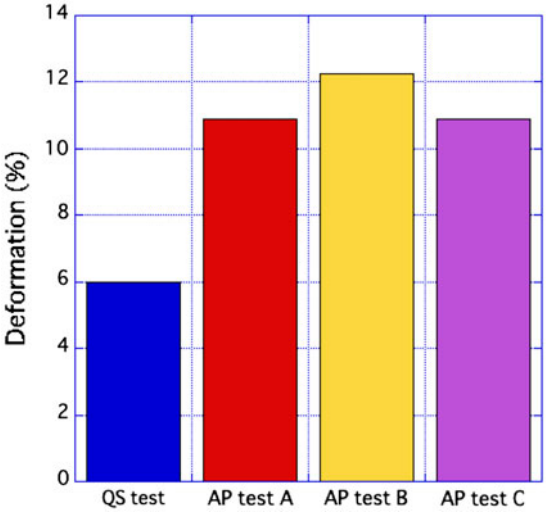

Figure 14. Deformations in the first slit layer after the arc-plasma wind tunnel heating tests compared with deformation after the quasi-static heating test.

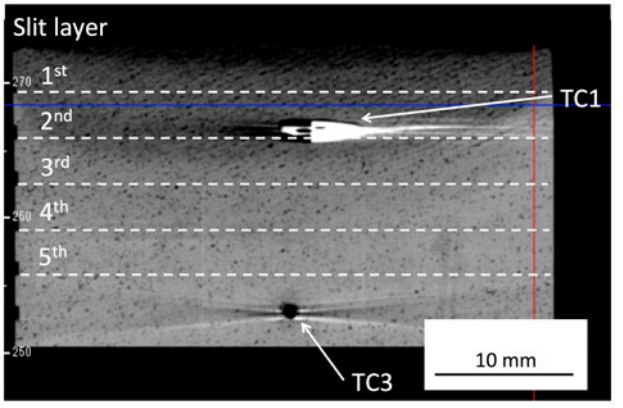

Figure 15. A cross-section of the Material 1 specimen after arc-plasma wind tunnel heating test *A* as observed using X-ray CT.

Figure 16 portrays a cross-section of the second slit layer after heating in test *C*. As this figure shows, cracks inside bundles, similar to that observed under QS, was also generated after the AP tests. Therefore, the buckling of fiber bundles is one of source mechanisms for the expansion in the AP tests.

In addition to the buckling defects, delaminations between laminae were observed after heating in AP test *C*, as presented in Figure 17. The delaminations expanded the thickness. Consequently the delamination caused by thermal stress was the reason producing the larger expansions in the AP tests. Rapid heating in the AP tests induced a steep temperature gradient inside the material. This temperature gradient produces high thermal stress, and likely engenders the delaminations. In contrast, only a few delaminations were observed after the QS test.

3.2.4. *Deformation temperature*

Table 6 presents the maximum temperatures measured by pyrometer, TC 1 and TC 2. TC 1 was located closed to boundary between the first and second slit layers, and TC

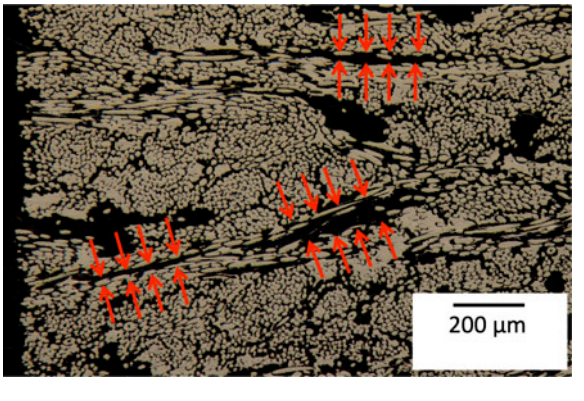

Figure 16. Typical optical micrograph of a cross-section observing the second layer obtained after arc-plasma wind tunnel heating test *C*.

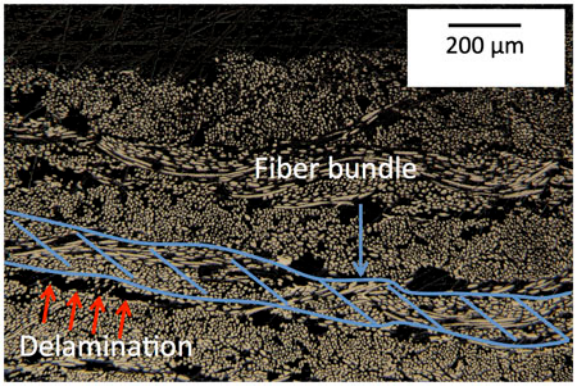

Figure 17. Optical micrograph of a cross-section in the first slit layer after arc-plasma wind tunnel heating test *C*.

Table 6. Maximum temperatures on the specimen surfaces of and in specimens attained in the arc-plasma wind tunnel heating tests.

AP test	*A*	*B*	*C*
Distance from the surface	Maximum temperature (°C)		
0.0 mm (surface)	2220	2593	2601
6.67 mm (TC 1)	955	Broken	Broken
13.3 mm (TC 2)	213	170	181

2 between the third and fourth slit layers. As Table 6 presents, the maximum temperature from the first to second slit layer, where the expansion occurred actively, was 955–2220 °C. The slit layers above the second layer in AP test *B* and *C* probably show

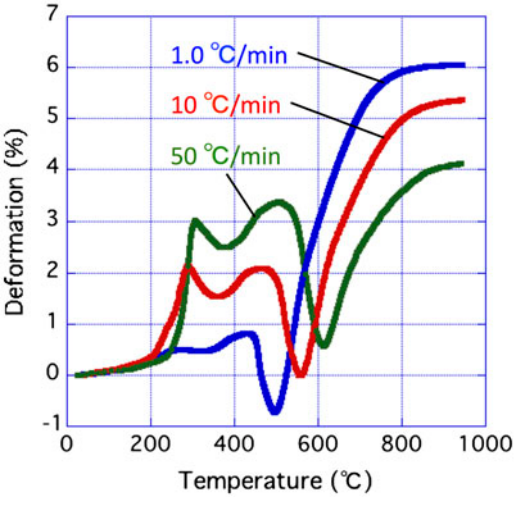

Figure 18. Effect of heating rate on thermal deformation of Material 1 obtained under quasi-static heating conditions.

high temperatures similar to that in test *A*. This means that the expansion deformation in the AP tests was induced mainly at temperatures higher than 900 °C. In contrast, the expansion in QS occurred in temperature range 500–900 °C, and no deformation was observed at temperatures higher than 900 °C. Accordingly, the temperatures producing active expansion deformation in the AP tests were higher than those obtained in the QS test.

Thermal deformations were measured at three heating rates under QS environments, and result is presented in Figure 18. This figure clearly shows that temperature starting the expansion becomes higher with increasing heating rate. At a high heating rate, the pyrolysis reactions cannot catch up with temperature raise, because it takes time until the pyrolysis reaction is completed. Because of this retardation effect, the temperature starting the cracking causing the expansion in the AP tests moved much higher than that in the QS test.

4. Conclusions

4.1. Quasi-static heating tests (QS tests)

When the material has small pores, the buckling of fiber bundles generated during pyrolysis reaction opens cracks wider and increases specimen thickness. In contrast, when large pores are included in the matrix, the cracking in the matrix relaxes the compressive stress in fiber bundles and suppresses buckling, and thus specimen thickness shrinks.

4.2. Arc-plasma wind tunnel heating test (AP test)

Results of the AP tests for Material 1 including small pores were compared with those of the QS test. The expansion of the thickness by AP became greater than that by QS, because delaminations were generated in addition to the buckling of fiber bundles.

The temperature generating expansion in AP was higher than that in QS, because heating rate in the AP tests was extremely high.

Acknowledgment

Our deepest appreciation goes to German Space Center (DLR), especially Dr Voggenreiter, whose corporations were inestimable value for our investigation using arc-wind plasma tunnel. Discussion with Professor Yasuo Kogo of Tokyou University of Science and Associate Professor Tetsuya Yamada of Institute of Aerospace exploration Agency was helpful to brush up the contents of present study.

Funding

This work was partly supported by JSPS Kakenhi (Grants-in-aid for Scientific Research (B)) [grant number 25289311].

References

[1] Yamada T, Ishii N, Inatani Y, Honda M. Thermal protection system of reentry capsules with superorbital velocity. ISAS Report SP. 2003;17:245–261.
[2] Inatani Y, Ishii N. Design overview of an asteroid sample return capsule. ISAS Report SP. 2003;17:1–15.

[3] Suzuki T, Sawada K. Thermal response of ablative test piece in arc-heated wind tunnel. In: 42nd AIAA Aerospace Sciences Meeting and Exhibit, AIAA 2004-341 2004 Jan 5–8; Reno, Nevada; 2004.
[4] Wittel FK, Schulte-Fischedick J, Kun F, Kröplin B-H, Frieß M. Discrete element simulation of transverse cracking during the pyrolysis of carbon fibre reinforced plastics to carbon/carbon composites. Comput. Mater. Sci. 2003;28:1–15.
[5] Schulte-Fischedick J, Seiz S, Lützenburger N, Wanner A, Voggenreiter H. The crack development on the micro- and mesoscopic scale during the pyrolysis of carbon fibre reinforced plastics to carbon/carbon composites. Compos. Part A. 2007;38:2171–2181.
[6] Schulte-Fischedick J, Zern A, Mayer J, Rühle M, Voggenreiter H. The crack evolution on the atomistic scale during the pyrolysis of carbon fibre reinforced plastics to carbon/carbon composites. Compos. Part A. 2007;38:2237–2244.
[7] Ogasawara T, Ishikawa T, Yamada T, Yokota R, Itoh M, Nogi S. Thermal response and ablation characteristics of carbon fiber reinforced composite with novel silicon containing polymer MSP. J. Compos. Mater. 2002;36:143–157.
[8] Herdrich G, Petkow D. High-enthalpy, water-cooled and thin-walled ICP sources: characterization and MHD optimization. J. Plasma Phys. 2008;74:391–429.
[9] Kubota Y, Kouhei K, Hatta H, Langhof N, Krenkel W, Kogo Y. Thermal deformation mechanisms of carbon fiber reinforced phenolic composites at elevated temperatures. Carbon. 2013;1:28.